Flow in meander bends with recirculation at the inner bank

Robert I. Ferguson and Dan R. Parsons[1]
Department of Geography, University of Sheffield, Sheffield, UK

Stuart N. Lane and Richard J. Hardy
School of Geography, University of Leeds, Leeds, UK

Received 3 January 2003; revised 8 August 2003; accepted 1 October 2003; published 21 November 2003.

[1] In highly curved river bends, flow may separate at the inner bank to create a recirculation eddy with weak upstream flow. Very little is known about how recirculation eddies connect with the downstream flow or how the latter is affected by their presence. We investigate these questions using three-dimensional time-averaged computational fluid dynamics models of two natural bends with inner-bank separation. Test measurements of velocity in one bend agree well with the simulation. Common points in the two simulations are that (1) an outer-bank helix is only present in the upstream part of the bend, (2) maximum near-bank velocities are highest here rather than beyond the apex as in most bends, (3) reverse flow extends farther across the channel at the surface than the bed, and (4) flow within the recirculation eddy has a three-dimensional structure, linked with that in the outer-bank free stream. Substantial differences in detail between the two bends appear to be due to differences in upstream planform, manifested through the lateral distribution of inflow velocity. *INDEX TERMS:* 1824 Hydrology: Geomorphology (1625); 1894 Hydrology: Instruments and techniques; 3210 Mathematical Geophysics: Modeling; *KEYWORDS:* CFD, bend, flow separation, recirculation, helical motion, dead zone

Citation: Ferguson, R. I., D. R. Parsons, S. N. Lane, and R. J. Hardy, Flow in meander bends with recirculation at the inner bank, *Water Resour. Res.*, *39*(11), 1322, doi:10.1029/2003WR001965, 2003.

1. Introduction

[2] It has been understood for over a century that the basic flow structure in a river bend is a helix. Faster near-surface flow moves toward the outer bank because the centrifugal acceleration acting on it exceeds the centripetal acceleration due to superelevation. The opposite is true for the slower-moving near-bed flow which therefore moves toward the inner bank. In laboratory bends of moderate curvature and symmetric cross section the helix occupies the full width. In natural bends it may be restricted to the outer part of the channel if a shallowly submerged point bar steers the inner-bank flow entirely outward [e.g., *Dietrich and Smith*, 1983; *Van Alphen et al.*, 1984; *Thorne and Rais*, 1985].

[3] In sharply curved bends another major flow structure is often present: a recirculation eddy generated by flow separation at the inner or outer bank. In this paper we investigate recirculation generated by high curvature of the inner bank, producing a "dead zone" of weak reverse flow immediately past the apex [e.g., *Rozovskii*, 1957; *Leopold et al.*, 1960]. Small recirculation eddies at the inner bank may also exist in the lee of emergent or shallowly submerged point bars [e.g., *Frothingham and Rhoads*, 2003]; they probably share some of the same features but are not the focus of this paper. However it is generated, flow separation alters the locations of strongest and weakest flow and thus has important implications for sedimentation and meander migration. The existence of a recirculation eddy or "dead zone" also creates a distinctive ecological niche and is likely to reduce flow mixing and pollutant dispersal. Yet very little is known about the detailed flow structure in bend recirculation eddies, how it links with the main downstream flow, or to what extent the latter retains the normal helical motion. *Hodskinson and Ferguson* [1998] simulated a field example fairly successfully using a three-dimensional (3-D) computational fluid dynamics (CFD) code, but neither they nor previous researchers described the flow structure in any detail.

[4] We have investigated flow separation along the inner banks of two sharp meander bends using a combination of fieldwork and modeling. Field measurements of velocity and turbulence were used to set up and test 3-D CFD simulations. Flow structures were then identified and described using the model output which, to the extent it is credible, is spatially much richer than field measurements can hope to be. In this paper we discuss technical issues in setting up CFD models of natural river bends with recirculation, validate the model on field measurements in one bend with a small recirculation eddy, then use it to investigate the detailed flow structure in this bend and another with a much bigger recirculation. The specific questions we seek to answer are: Can generic flow structures be identified in the two bends? Are there differences between the two bends, and if so what local factors appear responsible for them? What are the main differences between bends with and without separation? And how is the flow in an inner-

[1]Now at Department of Earth Sciences, University of Leeds, Leeds, UK.

0043-1397/03/2003WR001965$09.00

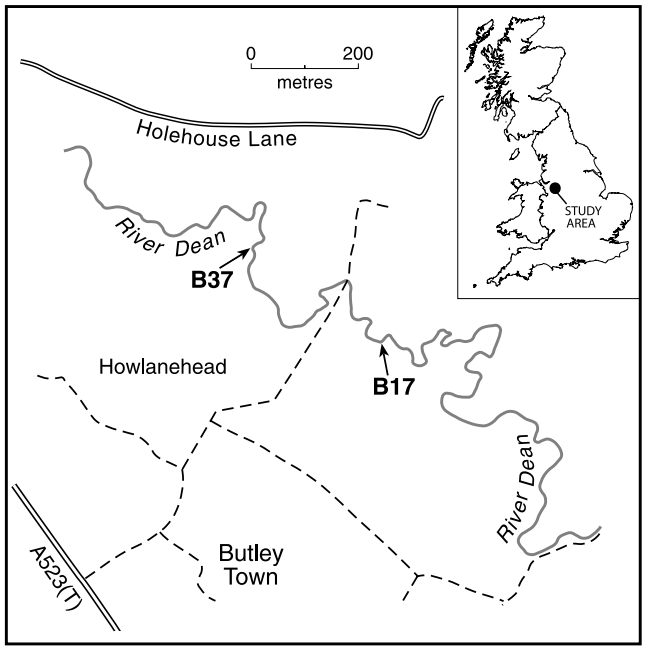

Figure 1. Location of study reach and of modeled bends within it.

bank recirculation zone linked with the downstream flow along the outer bank? The flow structure in a bend with recirculation at the outer bank will be addressed elsewhere, as will the dependence of recirculation in bends on discharge level.

2. Study Site and Field Measurements

2.1. Study Site

[5] The bends studied in this paper are close together on the River Dean, which flows across the glacial sediments of the Cheshire Plain just south of Manchester in northern England (Figure 1). The Dean is actively meandering with well-developed pool-riffle morphology. Its bed and banks consist mainly of gravel but with sand on sheltered parts of point bars and in recirculation zones, and a drape of silty sand on the bank tops. It has an active floodplain that is slightly incised into the main glacial plain, so that the channel is locally confined by low (1–3 m) terraces that restrict an otherwise freely meandering habit. The selected bends are not affected by tree roots or large woody debris, though others are. The hydrological regime is fairly flashy with flood events generated mainly by autumn and winter frontal rainfall but also summer convective storms. Bank-full discharge in the study reach is 2–3 m^3s^{-1}; bank-full width is typically 4–5 m but varies between 3 and 10 m.

[6] In order to assess the frequency of flow separation, the second author inspected all bends in accessible reaches of the stream from where it leaves the hills to where it joins the larger River Bollin. Flow separation at one or both banks was observed in nearly half of the 411 bends identified, with inner-bank recirculation extending at least a quarter of the way across the channel in 9% of all bends and halfway across the channel in 2% [*Parsons*, 2003]. Inspection of larger streams in the area showed a similarly high frequency, and we understand separation is also common in lowland streams in the United States [*Frothingham and Rhoads*, 2003; B. Rhoads, personal communication, August 2001]. Two representative bends with inner-bank separation were selected for modeling. Bend 17 has a small recirculation eddy. Bend 37, previously studied by *Hodskinson and Ferguson* [1998], has an unusually large recirculation eddy extending most of the way to the outer bank. The positions of the bends within the meander train are shown in Figure 1.

2.2. Topographic and Flow Measurements

[7] Measurements in bend 37 were made in August 1995 at a time of fairly low and almost steady discharge. The field methods are described by *Hodskinson and Ferguson* [1998]. In brief, the topography was quantified by surveying 12 cross sections, more closely spaced in the sharpest part of the bend. Streamwise and lateral velocity components were measured at the inflow and selected other sections using an electromagnetic current meter, and a bed-surface grain size distribution was measured by pebble count near the inflow. The topographic, roughness, and inflow data are used below to set up a new CFD model. The within-bend velocity measurements are used to delimit the recirculation as a test of the model, but no further validation is attempted because these velocity data are only 2-D and of coarser spatial and temporal resolution than we subsequently obtained in bend 17.

[8] Bend 17 was investigated in July 2000, again at fairly low and almost steady discharge. Its topography was surveyed by total station using breaks of slope to define primary features and spot heights to add detail (404 points in all). These data were used to construct a digital elevation model (DEM). The water surface elevation at many points within the submerged area was obtained by recording the vertical angle to the intersection of the reflector rod with the water surface. The surface extent of the recirculation eddy was also mapped. Size counts of 100 surface pebbles were made in 1-m^2 quadrats at several locations in the bend to help specify bed roughness. Velocity measurements were made to obtain inflow boundary conditions and spatially distributed validation data. The measurements were made using a Sontek™ acoustic Doppler velocity meter (ADV) mounted on a specially made wading rod. This had an attached spirit bubble to ensure the rod was vertical, and a pair of reflectors on a crossbar which were surveyed from the total station to fix the location and orientation of the ADV probe in the same coordinate system as the DEM and CFD model (see *Lane et al.* [1998] for details). The ADV measures three orthogonal components of velocity at 25 Hz in a sensing volume of <1 cm^3 about 5 cm below the probe. Inflow measurements were made for 120 s at each of several heights every 0.25 m across the channel. These data were used to calculate stream discharge and interpolate the inflow velocity distribution as a boundary condition for the CFD model. Test data were collected by fixing the ADV at one height and recording for 60 s at each of a number of locations 1–2 m apart throughout the bend, then doing the same with the ADV set at a second height. This procedure does not generate vertical or lateral velocity profiles of the kind commonly used to test simulations of laboratory flows, but for our field sites and equipment it was quicker than profiling and thus allowed the collection of more data before there was a significant change in water stage (which fell by only 4 mm during the flow measurement period). It also meant that test data were obtained

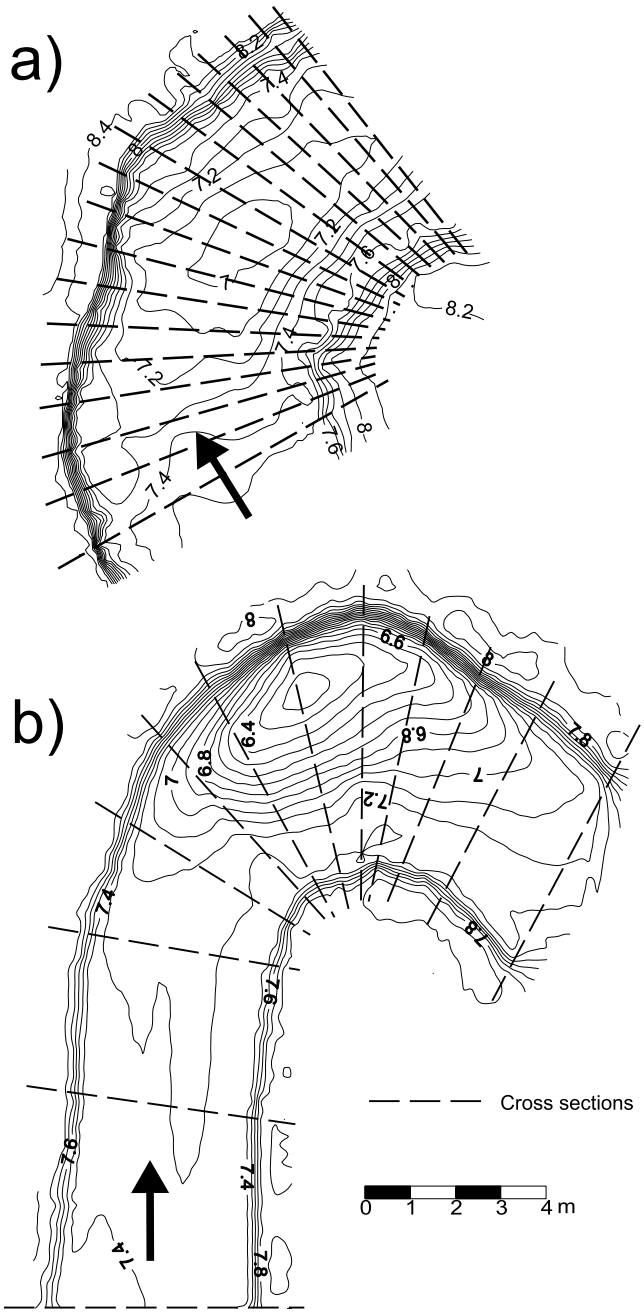

Figure 2. Topography of the two study bends as determined by field survey and kriging, and cross sections used to interpolate boundary-fitted CFD grids. Cartesian coordinate system for Figure 3 and Tables 1 and 2 has x positive rightward along first cross section.

throughout the bend, and at a range of relative heights within the flow, rather than being concentrated in certain locations. The signal-to-noise ratio and correlation coefficient were used to check the quality of the velocity measurements. Mean velocities were computed and the series were subject to a low-pass Gaussian filter [*Lane et al.*, 1998] before turbulent kinetic energy (TKE) was calculated.

2.3. Bend Morphology

[9] Bend 17 (Figure 2a) is a fairly sharp bend which turns 80° to the right over a centerline distance of 10 m. The channel has a bank-full width of 5–6 m so the mean ratio of radius of curvature (R) to width (W) is about 1.4. Total relief from the left-bank floodplain to the deepest part of the pool (near the centerline and past the apex) is 1.4 m. The left, outer bank is 0.9 m high and eroding over its full length. The right, inner bank is less steep and is vegetated down to the low-flow waterline. Neither bank is uniformly curved in plan. The inner bank follows the common pattern of being sharpest at the apex, and the outer bank has a slight reverse curve opposite the apex separating two zones of fairly high curvature. This irregularity in outer-bank curvature does not appear to be due to any variation in bank materials, so probably reflects the location and size of cantilever failures of the more cohesive upper bank as the basal gravel is eroded during floods. Remains of collapsed blocks are responsible for local irregularities in the bed topography near the left bank downstream from the pool. Flow enters over a gravel riffle. This is highest in midstream so there are two talwegs, that on the left being deeper. The mean flow depth varied considerably around the bend, from a maximum of 0.34 m at the inflow to 0.76 m in the pool and 0.51 m at outflow from the bend. The central and outer parts of the bed are gravel throughout, with D_{84} ranging from 69 mm on the riffle to 54 mm in the pool, but most of the small point bar at and beyond the apex of the inner bank is sand.

[10] Bend 37 is a sharp right-hand bend with a deep pool toward the outer bank and a small submerged point bar (Figure 2b). It follows a long, almost straight, riffle and leads immediately into a left-hand bend. The pool and its eroding outer bank consist of gravel but the point bar is sand-covered. The inner bank is grassed down to the normal waterline. The outer bank is capped by overbank fines with a grass root layer. When surveyed in 1995 bend 37 turned 130° to the right over a distance of 15 m along the outer bank and 7 m along the inner bank. These figures together with the mean channel width of 5.5 m give mean R/W ratios of 1.2 and 0.6 at the outer and inner banks. At the time the fieldwork was done the high curvature led to inner-bank separation which extended most of the way to the outer bank. By 2001 the outer bank had retreated substantially, increasing the radius of curvature, and the separation zone was less extensive. The upstream riffle and outer parts of the bed are gravel throughout, with a D_{84} of 66 mm, but most of the bed within the separation zone is sand.

3. Flow Modeling and Validation

[11] The CFD modeling was based on version 3.4 of the PHOENICS™ code, which solves the full 3-D Navier-Stokes equations discretized over a finite-volume grid. Following *Lane et al.* [1999], we used a hybrid-upwind numerical interpolation scheme which takes central differences between cells where diffusion dominates but upwind differences where convection is high (Peclet number >2). This is strictly only first-order accurate, but it is more stable than higher-order schemes which can introduce spurious oscillations into solutions. The hybrid scheme should give better interpolation within recirculations and dead zones while retaining second-order accuracy and low numerical diffusivity in the parts of the domain with fast downstream flow. Our spatially distributed validation data allow us to check the accuracy of the scheme in both situations. As solution accuracy controls sensitivity to grid design, we

undertook a rigorous grid independence test (see below). The pressure and momentum equations are coupled though the SIMPLEST algorithm [*Pantankar and Spalding*, 1972]. The solution was deemed to have converged when mass and momentum flux residuals were less than 0.1% of the inlet flux and spot values in a critical part of the domain were changing by less than 0.01%.

[12] Direct solution of the Reynolds stress terms in the Navier-Stokes equations cannot be accomplished for natural channel flows with currently available computer power. Here we use Reynolds averaging, and specifically the two-equation k-ε model modified by renormalization group theory [*Yakhot and Orszag*, 1986]. This allows greater dissipation in areas of high strain (as found in shear layers and separation zones), and tends to predict reattachment points better [*Yakhot et al.*, 1992; *Lien and Leschziner*, 1994]. It was independently chosen for all three of the pioneering applications of 3-D CFD to natural channels with complex geometry [*Hodskinson and Ferguson*, 1998; *Lane et al.*, 1999; *Nicholas and Smith*, 1999].

3.1. Computational Grid

[13] A boundary-fitted curvilinear computational grid was fitted to the irregular bend topography by specifying a series of cross-section planes, then interpolating more planes to define a grid with specified numbers of cells in the streamwise, transverse and vertical directions. The surveyed cross sections were used for bend 37. For bend 17 we extracted a series of 17 cross sections from the DEM, which gave greater freedom in the position of each cross section. The sections used for grid construction are shown in Figure 2a. Rapid changes in cell aspect ratio or orientation were avoided in the interests of numerical stability.

[14] The bend 17 model had 96 cells longitudinally, 42 across, and 10 vertically. Cells in the vertical were set so as to satisfy the dimensionless wall height (z^+) criterion:

$$30 < z^+ < 300 \tag{1}$$

where

$$z^+ = \frac{\sqrt{\tau_b/\rho}}{\upsilon} z_b \tag{2}$$

and τ_b is the bed shear stress, υ the kinematic viscosity, and z_b the distance between the center of the grid cell next to the wall and the wall itself. With this criterion, and the domain extent, this implies average cell dimensions of about 12 $\times$ 12 $\times$ 6 cm at the outer bank. Mean cell length decreases across the channel to $\sim$6 cm at the inner bank, and cell height varies between $\sim$1 and $\sim$9 cm according to local flow depth. From (2), reducing the thickness of the near wall cell further, by increasing the number of cells in the vertical, increases the possibility that the dimensionless wall height criterion is not met in areas of shallower flow. This limits the number of cells in the vertical. Two slight changes to the geometry of the inner bank had to be made before converged solutions could be obtained: rounding off the apex by 10 cm to avoid excessive change in direction at the apex section, and making the sloping grassy bank beyond the apex vertical for at least 5 cm at the waterline to avoid vanishing cell heights.

[15] The bend 37 model had 80 $\times$ 30 $\times$ 10 cells, with mean dimensions of $\sim$28 $\times$ 18 $\times$ 5 cm at the outer bank.

3.2. Boundary Conditions

[16] The necessary boundary conditions relate to inflow, outflow, wall treatment, and water surface. Distributions of velocity across the inflow plane were interpolated from the field measurements described above, using linear interpolation laterally and the law of the wall vertically. Bend 17 immediately follows another bend, so the model domain begins at the start of the bend and TKE at the inlet had to be measured. Bend 37 is preceded by a straight reach, so we could define an inlet well upstream of the sharp part of the bend, set inflow TKE to a nominal value, and allow the computed flow to evolve before the bend. A hydrostatic pressure distribution was applied to cells at the outlet plane. Pressure values within the domain are calculated relative to this, so the outlet planes need to be clear of the effects of negative dynamic pressure in areas of reverse flow. This was easy to achieve in bend 17 which is followed by an almost straight reach, but harder in bend 37 which leads directly into a reverse bend. Bed and bank roughness was parameterized using *Launder and Spalding*'s [1974] non-equilibrium version of the law of the wall in the layers of cells touching the rough boundaries. Shear further from the boundaries is modeled explicitly. A uniform roughness height was adopted, estimated from the riffle bed grain size distribution using $k_s = 3.5D_{84}$. This exaggerates the skin roughness of the sandy parts of the bed, but the sand was rippled which adds some form resistance that is not represented in the model grid geometry. Use of a gravel roughness is appropriate for the cut banks that are gravelly throughout, and is probably reasonable for those banks that were not eroding since they were all vegetated.

[17] The treatment of the free surface follows *Bradbrook et al.* [2000a]. Until recently most numerical models of open channel flow, including *Hodskinson and Ferguson*'s [1998] simulation of bend 37 using a different CFD code, specified a rigid lid at the free surface, across which all normal resolutes are set to zero. In practice, water surface elevations will deviate from this, especially where there is streamline curvature. The rigid lid treatment deals with the effects of this upon the momentum equations explicitly by introducing a nonzero pressure term at the surface [e.g., *Leschziner and Rodi*, 1979] to represent the effects of any superelevation or depression. It is also necessary to correct the mass continuity equation to recognize that the vertical extent of the flow domain also varies in the presence of deviation from the horizontal lid. If this is not done, velocity will be overestimated in zones of superelevation and underestimated in zones of depression. Thus we modified the code to correct for mass continuity effects by allowing variable porosities in the surface layer of cells (in effect, allowing the cell height to vary) so that mass continuity is maintained without distorting the streamwise velocity.

3.3. Solution Error, Grid Independence, and Validation

[18] The uncertainty in simulated flow properties in each bend can be estimated using the grid-convergence-index (GCI) method based on Richardson extrapolation [*Roache*, 1997; *Hardy et al.*, 2003]. We reran both models with the number of cells in each direction doubled and then halved. Table 1 shows the root-mean square differences between

Table 1. Root Mean Square Percentage Differences Between Simulated Flow Variables at Common Points of Coarse (C), Medium (M), and Fine (F) Grids in the Two Study Bends[a]

Bend	Grids	*u*	*v*	*w*	*k*
17	C and M	15	15	25	37
17	M and F	5	4	15	21
37	C and M	2	17	17	8
37	M and F	2	4	6	1

[a]Velocity components *u*, *v*, *w* are parallel to the field survey axes, not relative to the boundary-fitted coordinates of the flow model; *k* denotes turbulent kinetic energy.

simulated flow properties at common points of the three grids. With one exception (*w* in bend 17) all velocity components in both bends show little difference between medium and fine resolution predictions. This suggests the original medium-resolution velocity predictions were effectively grid-independent, and we therefore use them below to describe and illustrate the flow. However, TKE predictions (and those of *w* in bend 17) differ substantially between each grid which suggests the medium-resolution results are not grid-independent for these variables. Approximate 95% confidence intervals for flow properties on the medium grid, calculated by Roache's method, are mostly around ±10% (and narrower for *u* in bend 37), but considerably wider for *w* and *k* in bend 17.

[19] To confirm that the medium-resolution models reproduce measured flow properties to an acceptable accuracy we compared the bend-17 simulations with the 3-D ADV field measurements described above. The 2-D measurements in bend 37 were regarded as less reliable for this purpose, though *Hodskinson and Ferguson* [1998] found reasonable agreement with their fixed-lid CFD simulation of that bend. Recent open-channel applications of CFD have mostly relied upon qualitative comparison of model predictions with field measurements, often in the form of observed and predicted velocity profiles [e.g., *Czernuszenko and Rylov*, 2000; *Meselhe and Sotiropolous*, 2000; *Sofialidis and Prinos*, 2000]. However, *Lane and Richards* [2001] argue that this is not a sufficient test of a model as velocity measurements represent a sample of a much richer flow field and so formal inferential statistical testing of the agreement between predictions and measurements is required. We tested the present models using the time-averaged velocity magnitude at each of the 62 ADV measurement points in bend 17, and its Cartesian components *u*, *v* and *w* parallel to the survey axes. TKE was also compared, even though this paper is restricted to time-averaged flow properties, because its successful prediction would support the choice of turbulence model and because of its effects on mean flow estimates in areas of strong shear.

[20] Similar tests in the recent literature on CFD applications to open channels have reported r^2, the squared correlation between simulated and measured values of a flow property. In applications to smooth-walled flumes r^2 values of up to 0.95 for *u* and 0.75 for *w* have been achieved [*Bradbrook et al.*, 1998], but results for natural rivers show weaker agreement between model and measurement: r^2 values of 0.50–0.89 for velocity magnitude and its horizontal components, and 0.01–0.50 for *w* [*Hodskinson and Ferguson*, 1998; *Lane et al.*, 1999; *Nicholas and Smith*, 1999; *Bradbrook et al.*, 2000a; *Booker et al.*, 2001]. We obtain stronger agreement (as measured by r^2; Table 2) than in most of these previous studies, which gives some confidence in the use of the CFD results (rather than direct measurements) to identify and describe flow structures.

[21] A high correlation indicates small scatter rather than lack of bias, and this must also be checked [e.g., *Lane et al.*, 1999]. Thus we also inspected scatterplots of observed against simulated flow properties (Figure 3) and checked whether regression intercepts and slopes differed significantly from 0 and 1 respectively (Table 2). This test of bias is more sensitive for the relationships with high r^2 [*Lane and Richards*, 2001]. Error is possible in field measurements as well as CFD predictions so, unlike previous applications [e.g., *Lane et al.*, 1999] we fitted both forward and backward least squares regressions. The forward regressions ("CFD on ADV" in Table 2) are represented by the flatter of the two trend lines in each part of Figure 3. They are appropriate if error is assumed to exist only in the CFD predictions. The steeper ADV-on-CFD regressions are appropriate if error is entirely in the measurements, so these lines provide a limit to the range of possible fits. The results show no statistically significant bias in regression intercepts (and by implication no systematic error in mean values of simulated flow properties), nor in the slopes of backward regressions. However, the forward regression slopes are slightly (but significantly) lower than 1 for velocity magnitude and its horizontal components, and much lower for *w* and *k*. This means the CFD model tends to predict less spatial variability in flow properties than is present in the measurements. This is most obvious in the *w* plot (Figure 3d), where measurements range ~50% wider than predictions even though the latter have the right sign (i.e., whether flow is upwelling or downwelling) at all but a few points.

[22] Detailed inspection revealed that the main discrepancies in *u* and *v* are near the margins of the recirculation eddy. Figure 4 shows the mapped and simulated surface limits of recirculation in both bends. This reveals that the simulation of bend 17 underestimates the width of the proximal part of the recirculation by one cell and its upstream extent by two grid cells. None of the velocity measurements in this bend shows reverse flow (negative streamwise velocity relative to curved grid) where the simulation does not, or vice versa, but the imperfect prediction of the extent of recirculation evidently leads to errors in velocity magnitude and direction further out into the channel. The discrepancy is probably due to the need to

Table 2. Validation Results for Bend 17: Comparison of ADV Measurements at 62 Points With CFD Model Predictions[a]

	CFD on ADV			ADV on CFD	
Variable	*a*	*b*	r^2	*a*	*b*
u (m s^{-1})	0.01 ± 0.01	0.83 ± 0.08	0.90	0.00 ± 0.01	1.08 ± 0.10
v (m s^{-1})	0.01 ± 0.01	0.91 ± 0.08	0.89	0.01 ± 0.01	0.99 ± 0.08
magnitude (m s^{-1})	0.02 ± 0.02	0.82 ± 0.10	0.82	0.01 ± 0.02	1.01 ± 0.12
w (m s^{-1})	0.00 ± 0.02	0.37 ± 0.10	0.44	0.00 ± 0.00	1.19 ± 0.35
k (m^2 s^2)	0.00 ± 0.00	0.40 ± 0.12	0.43	0.00 ± 0.00	1.06 ± 0.32

[a]Forward and backward regression intercepts (*a*) and slopes (*b*) are shown, each with 95% confidence intervals and squared correlation coefficient (r^2). Flow variables *u*, *v*, *w*, *k* are as defined in Table 1; magnitude is calculated from all three velocity components.

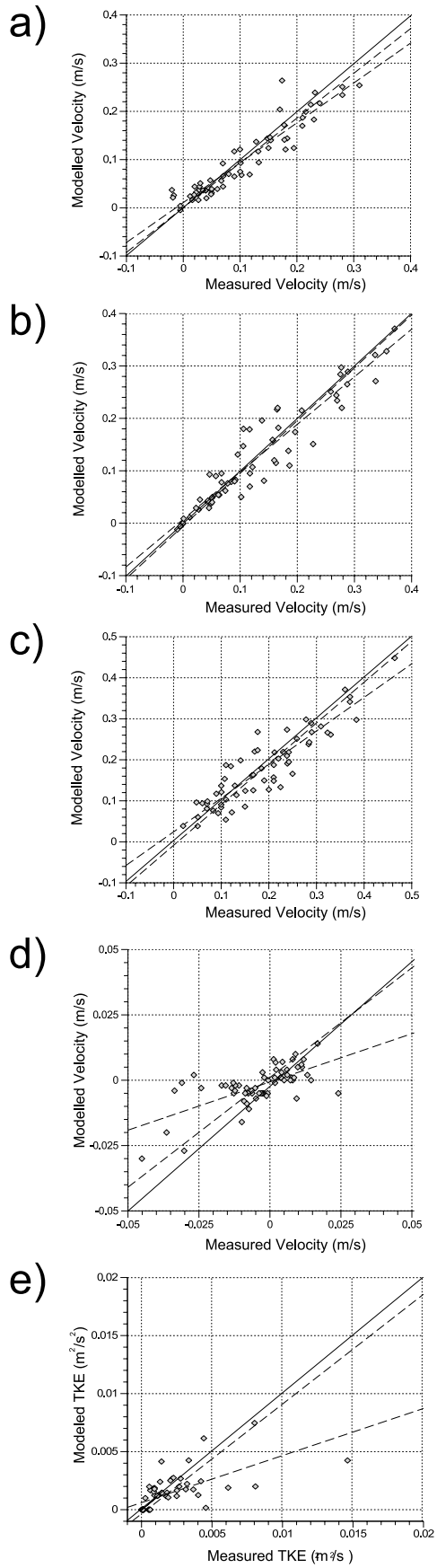

Figure 3. (opposite) Validation plots for bend 17. Flow properties measured by acoustic Doppler velocimetry (ADV) at 62 points are compared with CFD-simulated values at the nearest matching points. From top to bottom the plots show horizontal velocity components u and v, 3-D velocity magnitude, vertical velocity component w, and turbulent kinetic energy k. Solid lines are those of perfect fit; dashed lines are regressions using forward and backward least squares fits.

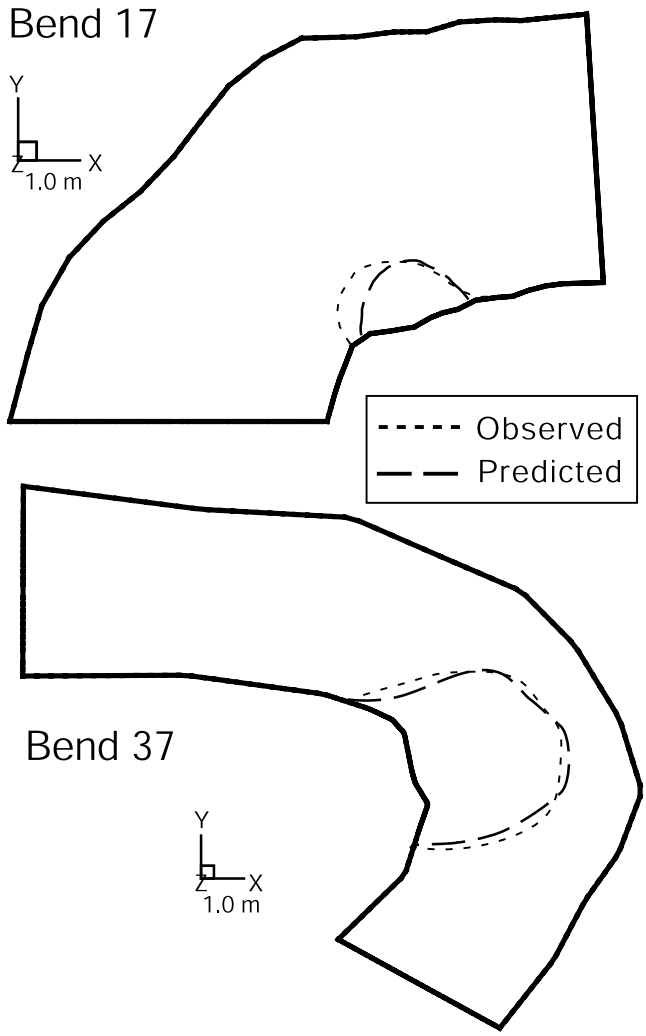

Figure 4. Observed and simulated limits of surface recirculation in the two bends.

round off the abruptness of the inner-bank apex. Underestimation of dead-zone width implies overestimation of the width over which flow is downstream, and thus a tendency to underestimate positive velocities in that part of bend 17. This may explain the small bias apparent in Figures 3a and 3b.

[23] The surface extent of the much bigger recirculation eddy in bend 37 is predicted extremely well (Figure 4), with a maximum error of one grid cell. In this bend, 21 velocity measurements revealed reverse flow and 20 of them are within the simulated recirculation; two measurements within the simulated recirculation showed small positive streamwise velocities. This shows excellent agreement in

the simulated extent of recirculation below the surface as well as at the surface.

[24] Reverting to the bend-17 validation in Figure 3, the biggest discrepancies in w are near the edge of the dead zone or the outer bank of the pool. Small measurement errors in w are possible because of the difficulty of holding the ADV wading rod exactly vertical, but measured values greater than ± 0.02 m s^{-1} are too big to be explained in this way. Errors near the edge of the dead zone could relate to macroturbulent structures in the shear layer, especially in view of the short duration (60 s) of each measurement. The outer-bank errors are probably due to bed irregularities not included in the model geometry: large protruding clasts which had presumably fallen in from the eroding bank, and must have deflected the flow to some extent. The main discrepancies in the TKE plot relate to drastic underprediction at a handful of points. These could also relate to macroturbulence near the shear layer or in the wake of large clasts on the bed.

[25] Although the CFD predictions do not always match perfectly with the measured velocity and turbulence values the agreement is generally good, and comparable to what has been regarded as acceptable by researchers modeling flume data [*Bradbrook et al.*, 1998; *Huang et al.*, 2002]. In view of the additional uncertainties of field data collection we therefore regard the model as adequately validated for use in discussing the large-scale flow structures present in the two bends.

4. Large-Scale Flow Structures

[26] Previous discussions of flow structures in meander bends, and in other channel features such as confluences and braids, have mostly been based on detailed field measurements at a number of cross sections [e.g., *Dietrich and Smith*, 1983; *Ashmore et al.*, 1992; *Rhoads and Kenworthy*, 1995]. Patterns of secondary circulation have generally been inferred from plots of cross-stream velocity, though not without controversy since such patterns can appear very different according to the orientation chosen to define the local streamwise direction [*Lane et al.*, 2000; *Rhoads and Kenworthy*, 1999]. Only very recently have 3-D velocity measurements been used [e.g., *Rhoads and Sukhodolov*, 2001; *Frothingham and Rhoads*, 2003]. Some authors have also [*Ashmore et al.*, 1992], or instead [*Van Alphen et al.*, 1984], mapped the difference in flow direction between surface and bed.

[27] By basing our discussion of flow structures on 3-D CFD simulations, validated against field measurements, we have spatially much richer information. Velocities are evaluated at $>10^4$ points in each bend, instead of $\sim 10^2$ in studies based entirely on field or flume measurements. The simulated values are of course liable to quasi-random error of the magnitude indicated in the last subsection, and may be systematically biased in certain localities (e.g., where the edge of the recirculation is mispredicted by one or two cells). Nevertheless, the broad patterns of flow are expected to be correct. The spatial richness of the simulations relates not just to the number of points resolved but also their near-uniform distribution in three dimensions throughout the bend. In contrast, cross-section-based field measurements are denser vertically than laterally and even sparser longitudinally. The high spatial resolution of the CFD models permits a wider choice of ways to visualize the results in order to identify, then describe and illustrate, flow structures. We inspected near-surface and near-bed vector and streamline maps; cross-section vector plots; contour maps of the streamwise (u), lateral (v), and vertical (w) components of velocity (defined hereafter relative to the boundary-fitted grid, not the DEM); maps of TKE and deviation from hydrostatic pressure; and vorticity plots. For illustrative purposes we use uv vector maps to show the spatial patterns of velocity magnitude and orientation, and vw vector plots to show secondary circulation in the plane of selected sections. The uv vector maps differ from the usual scaled-arrow plot in that we use unit arrows with velocity magnitude indicated by background isovels. This makes it easier to see flow directions in the extensive areas of very low velocity.

4.1. Horizontal Components of Velocity

[28] The simulated near-surface and near-bed flow patterns in both bends are shown in Figure 5, along with the locations of the sections used below to examine secondary circulation and for reference purposes in describing flow structures. Section A in each bend is on the face of the riffle just upstream of the sharp part of the bend. This is close to the inflow to the bend-37 model, but well downstream of the inflow to the bend-17 model. Sections C and D in each bend are near the apex and run through the inner-bank recirculation eddies and the deepest parts of the pools. Section F in each case is just downstream of the reattachment point. In bend 17 a final section (G) is marked in the near-straight exit region of the bend.

[29] The locally irregular geometry of these natural bends inevitably leads to a more complicated flow structure than in a laboratory channel or a CFD simulation of an idealized bend, but several large-scale features can be identified in each bend. Most are common to both bends, but there are some differences. We identify eight features in the results.

[30] 1. Although both bends have extensive areas of very slow flow, extending from the inner bank to well past the centerline, reverse flow is much more localized in bend 17 than in bend 37. The center of rotation of the recirculation eddy in bend 37 is more than halfway across the channel, whereas that in bend 17 is close to the inner bank. The fine detail of the recirculating flow structure is therefore more evident in bend 37 where it occupies far more of the bend. The reverse flow is strongest (>0.2 m s^{-1}) near the apex of the inner bank. The center of rotation is slightly further upstream and leftward at the surface than the bed, indicating that the axis of the recirculation vortex is not vertical. Likewise, reverse velocities extend further across the channel at the surface than the bed, indicating a non-vertical separation plane. There are hints of the same complexity in bend 17 but its recirculation eddy is too small to be resolved in comparable detail.

[31] 2. The velocity distribution entering bend 37 is almost symmetric, with maximum velocity in midchannel, but that entering bend 17 is asymmetric with the highest velocity near the left bank and a secondary maximum near the right bank. The existence of two filaments of high velocity is a site-specific feature which can be expected to complicate the flow structure in the rest of bend 17.

[32] 3. Despite the difference in extent of the recirculation eddies, flow separation and reattachment occur in about

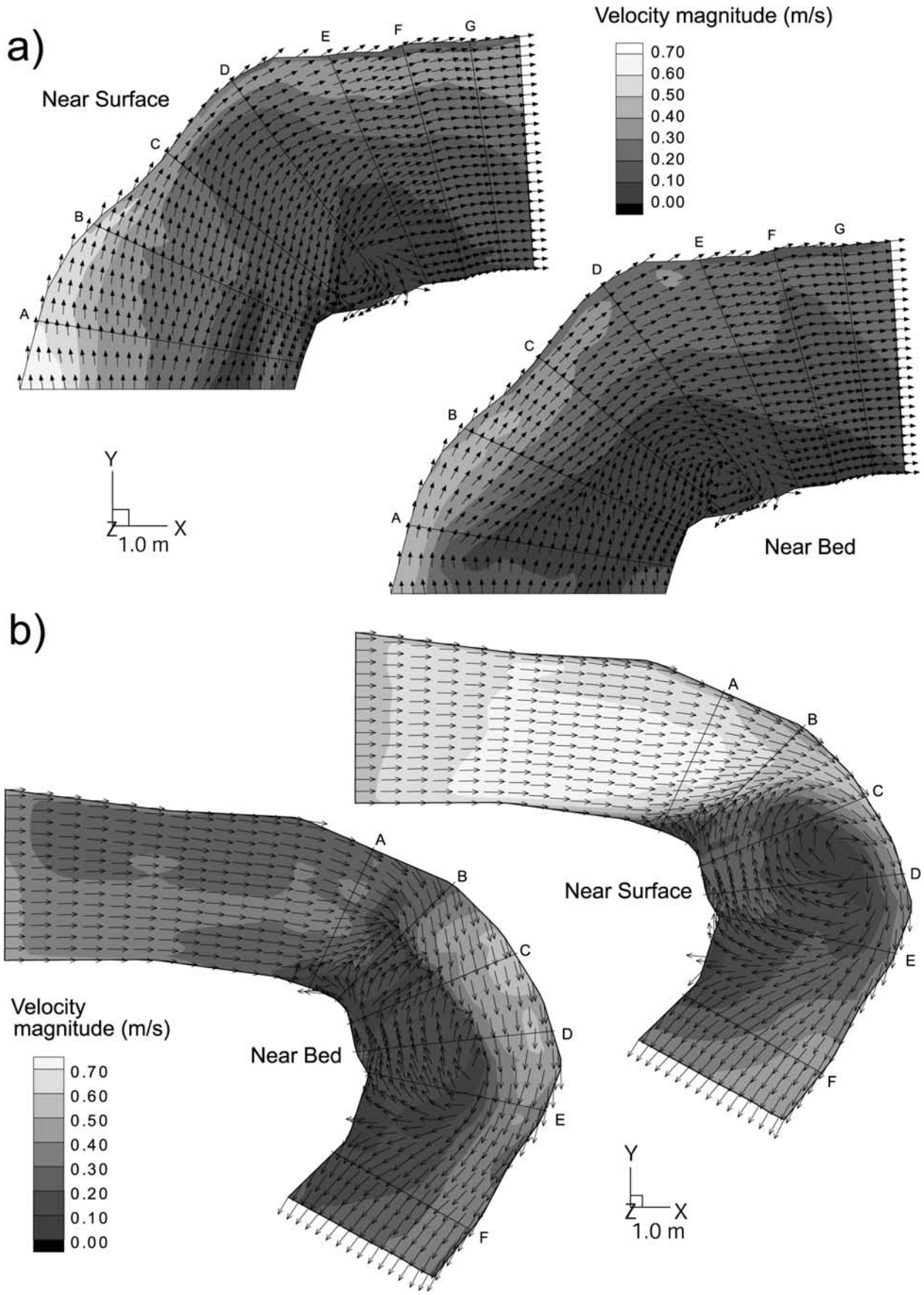

Figure 5. Simulated velocity distributions in the top and bottom layers of computational cells in the CFD models of the two bends. Contours show velocity magnitude, and arrows show flow direction. See color version of this figure in the HTML.

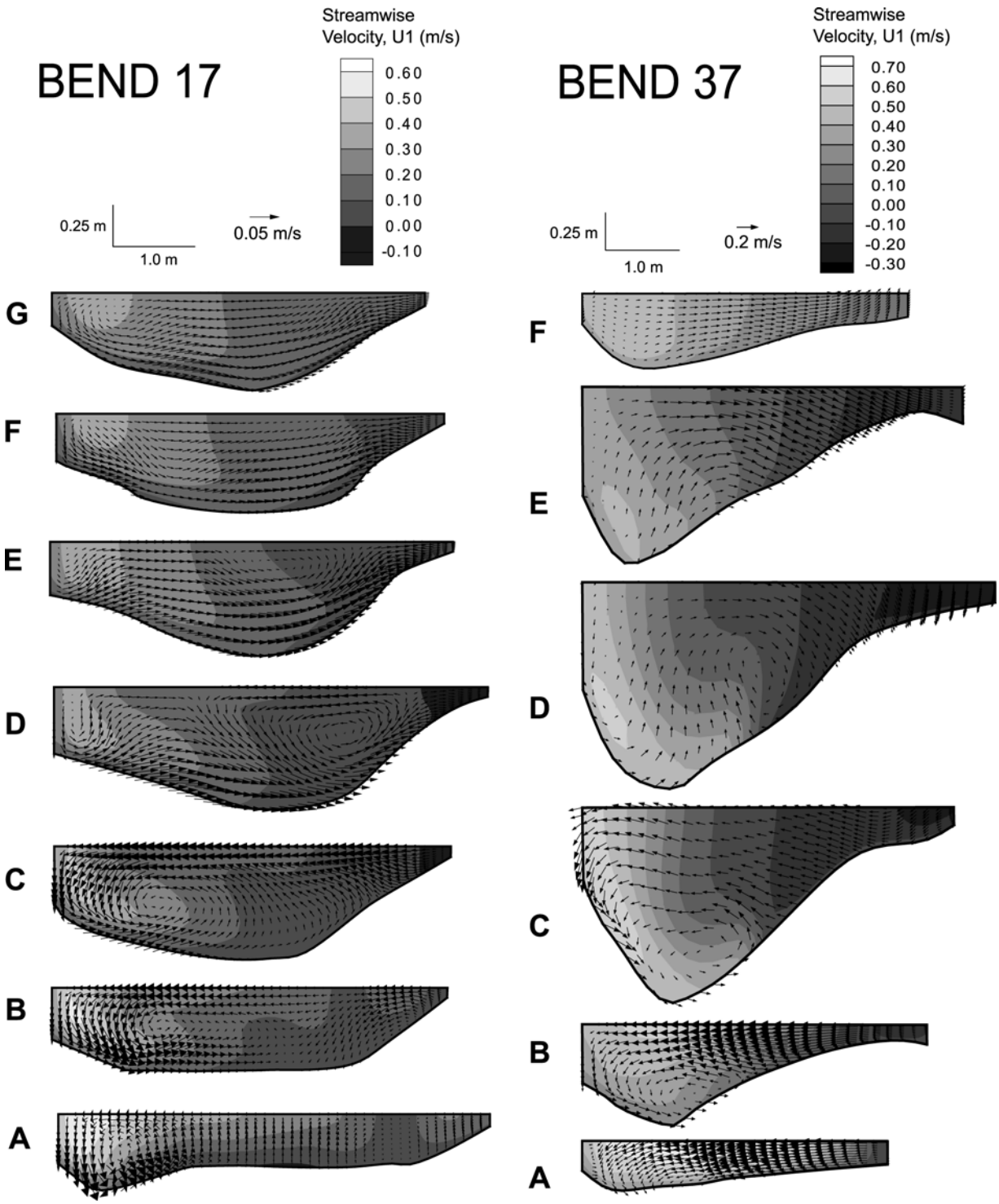

Figure 6. Simulated secondary circulation at selected cross sections of the two bends. Section locations are shown in Figure 5. Contours show streamwise velocity relative to CFD grid, and vectors show resultant lateral and vertical components. See color version of this figure in the HTML.

the same locations in each bend. Flow at both surface and bed separates from the inner bank at or just upstream from where it starts to turn sharply (near A in bend 37, between B and C in bend 17), then reattaches about midway from the apex to the end of the bend (between D and E in bend 17, E and F in bend 37). Flow near the separation and reattachment points is very slow, with velocity magnitude below 0.1 m s^{-1}, and pressure at mid-height in the water column is below hydrostatic at these locations.

[33] 4. The zone of reverse velocity is just the core of a more extensive "dead zone" of slow-flowing water. Taking the 0.2 m s^{-1} isovels in Figure 5 as arbitrary limits, both dead zones have maximum surface width rather past the apex (near section D in each bend). The pattern at the bed is

different: low velocities extend less far across at the apex, but occur further up and downstream, and extend furthest left proximally (near section A in bend 17, B in bend 37) where there is a big vertical velocity gradient in midstream.

[34] 5. There is substantial lateral asymmetry in the flow toward and around the apex of each bend, with the full-width inflow converging asymmetrically into an outer-bank free stream of considerably reduced width. This free stream must have a rather greater downstream water discharge than the stream as a whole, since it has to balance the upstream discharge near the inner bank. Velocities toward the outer bank are higher than those near the inner bank by a factor of 3 to 4, and along the proximal part of the outer bank the computed pressure at mid-height in the water column exceeds hydrostatic.

[35] 6. Despite the constriction of downstream flow into this relatively narrow free stream, there is a general deceleration of flow along the outer bank. This is due to the big increase in depth from the shallow inflow to the deep pool near the apex. Surface velocity near the outer bank falls by around 50% from inflow to apex in each bend, then increases slowly toward the shallower outlet. Bed velocity is more constant; in bend 17 it decreases a little, whereas in bend 37 it increases from <0.3 m s^{-1} at A and B to >0.4 m s^{-1} at C-E, then decreases toward the outlet.

[36] 7. Vector directions near the outer bank indicate outward flow at the surface, but inward flow near the bed, as far as the apex. The difference in direction is as much as 45° in places, and lateral velocities are high but of opposite sign at the surface and bed. This is indicative of a helical motion, as found in bends generally, but restricted here to the outer bank before the apex.

[37] 8. Beyond the apex, where the flow as a whole expands asymmetrically to reoccupy the full channel width beyond the dead zone, there is far less difference between surface and bed flow directions. This suggests rapid decay of the helix. Lateral velocities reach 0.2 m s^{-1} to the right between E and F in bend 37, but hardly any secondary flow remains at the final cross sections.

4.2. Vertical Velocity and Secondary Circulation

[38] Figure 6 shows secondary-circulation ($v\,w$) vectors and isovels of streamwise velocity (u) in the cross sections labeled in Figure 5. The plotted v components are relative to the orientations of the sections, which in turn are those of the boundary-fitted computational grid. These orientations do not necessarily yield zero cross-stream discharge in a section, let alone at a vertical, so helical motion (if present) might not be revealed by closed loops of vw vectors in the way that is inevitable when field measurements are reoriented to give zero cross-stream discharge at a vertical. However, it would still be revealed by differences in the sign of v at surface and bed, or differences in the magnitude of v at surface and bed combined with opposite signs of w on left and right.

[39] The plots confirm point 7 above: the existence of a strong outer-bank helix in the first half of each bend (sections A–C), with plunging at the bank and upwelling in midstream. As noted in points 5 and 6, its strength is enhanced by vortex stretching as the free stream narrows past the recirculation zone. This effect is, however, reduced by the increase in depth from riffle to pool. The cross-section isovels show that the fastest current becomes depressed below the surface, to the extent that the vertical velocity gradient is reversed in much of the outer part of bend 37. The axis of the vortex is well to the left of center throughout, so the plunging near the outer bank is much stronger than the upwelling on the midstream side of the vortex.

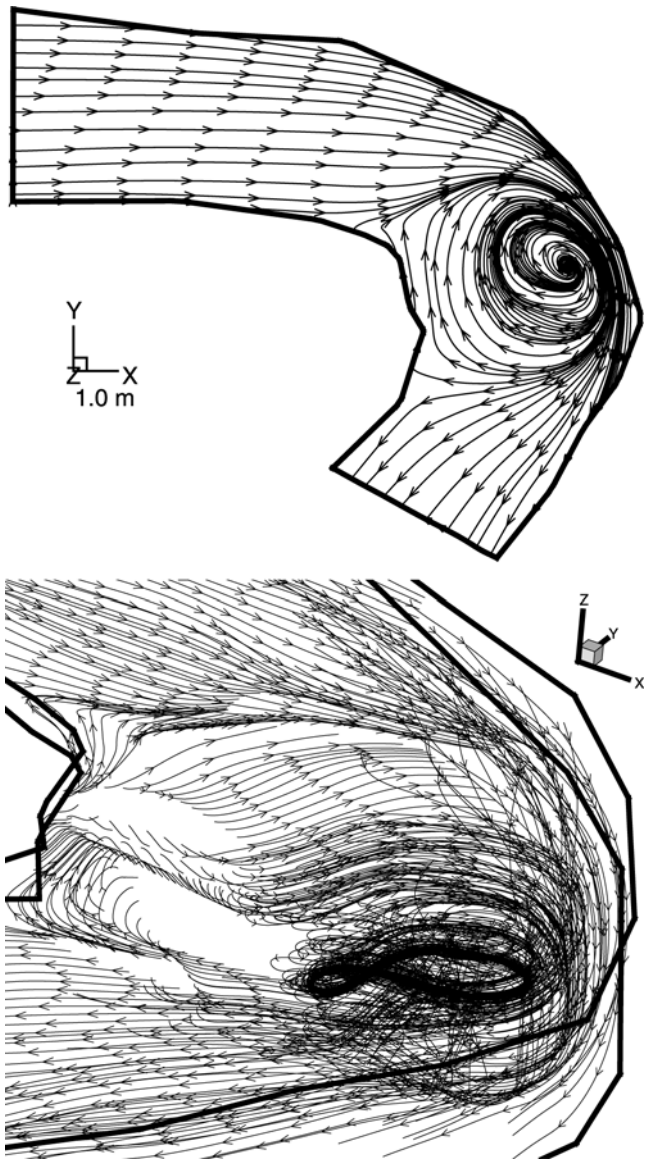

Figure 7. (top) Planimetric and (bottom) oblique views of selected streamlines in the simulation of bend 37 to show connections between free stream and recirculation eddy. Top map shows surface streamlines. Bottom view is looking upstream and downward, with the inner-bank apex on the left and the outer bank on the right.

[40] As noted in point 8, patterns of upwelling and downwelling weaken considerably beyond the apex of each bend. A decay in vorticity is to be expected as the cross-section area of the free stream increases past the recirculation. By section D in each bend the remains of the vortex can be discerned around the high-velocity core near the base of the bank, but the upwelling water nearer the surface no longer moves leftward toward the bank, and is shown as moving rightward at E and F. The impression of rightward

surface flow at E is entirely due to the nonorthogonality of this section to the outer bank of bend 17 (see the vectors in Figure 5), and is exaggerated in bend 37 for the same reason, but this is not a factor in either the lack of leftward flow at D or the presence of rightward flow at F.

[41] Visualization of streamlines from carefully chosen starting points in both bends revealed some interchange of fluid between the outer-bank helix and the inner-bank recirculation eddy. Figure 7 illustrates this for bend 37. The recirculation in bend 17 is impossible to show clearly because of its small size but shares some of the same features. The planimetric representation of surface streamlines in Figure 7 (top) confirms the separation and reattachment points inferred from the vector map in Figure 5. The three-dimensional view of selected streamlines in Figure 7 (bottom) reveals further detail, and two features in particular.

[42] 1. As the outer-bank helix decays past the apex of each bend, upwelling water on its right-hand side starts to escape rightward instead of spiraling leftward across the surface to the outer bank. This is suggested by the orientations of *uv* vectors in Figure 5 (between D and E in bend 17, between E and F in bend 37) and *vw* vectors in Figure 6 (sections D and E of each bend), and confirmed by some of the streamlines halfway across the foreground of Figure 7. These streamlines follow a hairpin path into the dead zone, starting with $u > 0$, $v \sim 0$, $w > 0$ but moving through $u \sim 0$, $v > 0$, $w \sim 0$ to $u < 0$, $v \sim 0$, $w < 0$. In bend 17, escape is not directly to the recirculation eddy but to the extensive dead zone of low positive u, within which there is another counterclockwise helix.

[43] 2. Streamlines within the extensive recirculation eddy in bend 37 show complex paths involving upward and downward movement as well as circulation in plan view. Flow is generally inward and downward distally (sections D and E in Figures 5 and 6) but outward and upward proximally (section C) where streamlines starting in the reverse flow near the inner bank are reentrained into the free stream, making an upstream-to-downstream hairpin turn (toward top left of Figure 7). This is hinted at in Figure 6 in the way the secondary vectors near the point-bar slope merge into the outer-bank helix. The same can be seen nearer the inner bank of section C in bend 17.

5. Discussion

[44] The spatial structure of time-averaged flow in real river bends is inevitably more complicated than that in idealized laboratory experiments or CFD simulations. Both the channel geometry and the inflow velocity distribution are less regular in the field than in the laboratory, so questions arise as to which flow features are generic to a class of bends and which are specific to a particular configuration. Some insight can be gained by looking at the similarities and differences between the two bends we have modeled, and the differences between their common features and those of the flow in ''classical'' bends without separation and recirculation.

[45] The defining feature of the flow structure in this class of bends is separation and reverse flow at the inner bank. Flow separates near the most sharply curved point on the inner bank, and the expansion zone past the apex contains a recirculation eddy (RE below) with a near-vertical axis of rotation. The REs in the two right-hand bends studied here rotate clockwise when looking downward, but the circulation would be counterclockwise in a left-hand bend. Downstream flow reattaches to the inner bank within about one channel width, but a dead zone of small downstream velocity extends further upstream and downstream at the bed. Both bends have very low radius of curvature relative to channel width, and the primary cause of separation appears to be the abruptness with which the inner bank changes direction. The momentum of the near-bank flow causes it to continue in a fairly straight path, leaving a zone of low velocity in what is effectively a sudden lateral expansion. A second aspect of the morphology of both bends is a pronounced deepening of the channel from the inflow riffle to the apex pool. This might promote separation by reducing mean velocity and momentum toward the apex and providing more room vertically for secondary circulation. This speculation could be tested by further CFD simulations with the same planforms but different long profiles.

[46] The other dominant feature in both bends is a free stream which runs along the outer bank, outside the RE, and exhibits helical motion. The outer-bank helix (OBH below) is counterclockwise looking downstream, so that surface flow is toward the bank and near-bed flow away from the bank. The OBH has the same curvature-induced origin as in meander bends without recirculation: fast surface water impinges on the bank to create superelevation which drives an inward near-bed flow. However, there are three distinctive (though not unique) features about the free stream and its helicity.

[47] First, the helical motion is restricted to the outer part of the channel. This can also happen through topographic steering over a point bar [as first described by *Dietrich and Smith*, 1983], but seldom if ever to the extent that helicity is restricted to only a quarter of the width as at the apex of bend 37.

[48] Second, the plunging at the outer bank before the apex is so strong that the highest velocities are depressed progressively nearer the bed. Submergence of the high-velocity core is not unknown in meander bends [*Bathurst et al.*, 1979; *Frothingham and Rhoads*, 2003], and is also characteristic of confluences with flow separation [*Rhoads and Kenworthy*, 1995], but it is unusually pronounced in bend 37 where the fastest flow is below mid-height at D and near the talweg at E, giving a reversed vertical velocity gradient.

[49] Third, the OBH is strongest proximally, where the bulk of the incoming flow converges on the outer bank not just passively as the bank starts to turn but also through the deflecting effect of the inner bank RE. At the apex the helix is restricted to a relatively narrow strip along the outer bank, where there is strong downwelling, but beyond the apex the helix first weakens and then disappears. This is different from the usual situation in less sharply curved bends, where the helix in one bend is generally regarded as surviving into the next before being replaced by one rotating in the opposite direction [e.g., *Thorne and Hey*, 1979]. It also contrasts with *Leeder and Bridge*'s [1975] discussion of inner-bank separation in bends of intertidal creeks: they speculated that maximum velocity and bank erosion

occurred in the distal half of a bend where the effective flow width is reduced past the recirculation eddy, whereas we find it further upstream because the reduction in effective width is more than offset by the increase in depth from riffle to pool. The rapid weakening of the OBH in our study bends is enhanced by vortex stretching as the free stream diverges asymmetrically to reoccupy the whole width of the channel past the distal end of the RE. This suppresses the secondary circulation, so that the flow at the bend exit is essentially parallel. *Frothingham and Rhoads* [2003] similarly found that helicity generated in the first sharply curved part of a compound bend decayed completely as the free stream expanded toward the inner bank past a point bar.

[50] The conjunction of the two main vortices (RE and OBH) gives pronounced lateral asymmetry in streamwise velocity toward and past the apex of each bend. Thus there is strong shear between relatively fast downstream flow near the outer bank and slow downstream or reverse flow nearer the inner bank. In the time-averaged CFD simulations described here, connections between the OBH and RE are to be found up and downstream of the latter. At its distal end, upwelling fluid on the midchannel side of the OBH escapes into the low-velocity, low-pressure zone toward the reattachment point inner bank and is turned upstream; then on approaching the separation point upstream of the apex, fluid is entrained back into the upwelling side of the developing OBH to complete a double-hairpin loop of recirculation. However, our field observations suggest there is also direct mixing across the essentially longitudinal shear zone between the OBH and RE, with frequent shedding of small Kelvin-Helmholz vortices. Such vortices have been reported from sharp bends in intertidal creeks [*Leeder and Bridges*, 1975] and from shear zones at confluences [e.g., *Biron et al.*, 1993; *Bradbrook et al.*, 2000b; *Sukhodolov and Rhoads*, 2001]. Strong turbulent diffusion in this manner may also be a further factor in the rapid weakening of the OBH past the apex of each bend.

[51] The main difference between the two bends is the much smaller extent of the recirculation eddy in bend 17. This probably relates mainly to the lower angle of turn and less extreme R/W ratio of this bend compared to bend 37. Nevertheless bend 17 still has an extensive dead zone, because although the RE is small it is separated from the OBH by a wide midchannel area of low downstream velocity. Thus there are two shear layers in this bend: a main one at the mid-channel side of the outer-bank free stream, and a milder one between the slow flow in the center of the channel and the reverse flow close to the inner bank. As noted in paragraph 42 and seen in Figure 6, particularly at D, the zone of slow downstream flow contains an counterclockwise secondary circulation. This probably reflects the asymmetric inflow to this bend, fastest near the left bank, slowest in midstream, and of intermediate velocity near the right bank. The left-bank jet leads into the OBH but the inner-bank separation and RE is created by the tendency of the right-bank inflow to continue straight on, diagonally across the channel through the low-velocity zone in midstream, through a combination of high inner-bank curvature and topographic steering by the small point bar that is present at the apex. This right-bank jet is eventually deflected rightward as it converges on the OBH. Since this happens further downstream at the surface than at the bed (because of the difference in orientation between near-bed and near-surface flow in the OBH), an overturning motion (counterclockwise vw vorticity) is imparted to the jet. We think this more complex pattern is a site-specific outcome of the unusual inflow to bend 17, and that the simpler flow structure in bend 37 is more generic.

[52] The intensity of recirculation in the latter bend is such that the RE extends into the path of the incoming flow, thereby deflecting it. This is an important difference between the two bends, and shows how separation can generate hydrodynamic phenomena of sufficient strength not only to maintain their spatial structure in the face of strong free stream flow, but also to influence the geometry of the free stream flow (as seen particularly in the deflection of surface flow vectors in Figure 5).

6. Conclusions

[53] The flow structures in these two bends share many generic features but exhibit some contingent differences. The generic features are a recirculation eddy at the inner bank and a free stream at the outer bank within which helicity first increases, then decays through vortex stretching. The controlling factors for the development of these phenomena seem to be high channel curvature, inflow distribution to the bend, and bed topography. We regard high planform curvature as a generic factor, necessary for separation to occur. The inflow distribution is a modifying factor giving site-specific differences between bends, enhancing or diminishing the pressure gradients induced by curvature according to the angle at which flow impinges on the outer bank and the speed of the flow past the inner-bank apex. The pronounced riffle-pool bed topography of the River Dean is a contributory factor to some of the common features of the study bends, and is probably a factor in the extent of the recirculation eddy in bend 37, but it is not a necessary condition for recirculation (which has been observed in laboratory channels without pools and riffles). Once recirculation has developed, the dead zone acts as a fourth factor, modifying the flow structure through the interaction and shear between the region of much slower or reverse flow close to the inner bank and the free stream near the outer bank.

[54] The presence and nature of recirculation may alter with flow stage as the relative influence of these controlling factors varies. For example, the influence of the upstream riffle bed topography is likely to reduce as discharge increases. Our field observations suggest that large recirculation eddies exist even in high flows, and in ongoing research we are investigating this by running validated CFD models at higher discharges.

[55] The existence of large areas of slow downstream or reverse flow in bends like these has important implications. The velocity patterns discussed above imply maximum boundary shear stress near the outer bank, as in the classical model, but upstream of the apex rather than downstream of it. This has implications for bank erosion and meander migration, and may also be a precursor to the development of outer bank flow separation. The inner-bank zones of slow flow also severely affect the sediment dynamics of the system and act to accumulate patches of fine sediment. Our results show that CFD models can be fitted successfully

to bend flow with separation, so they offer a valuable new tool for investigating the implications of separation.

[56] **Acknowledgments.** This research was funded by the UK Natural Environment Research Council (grant GR3/9715 to Lane and Ferguson). We thank the local farmer (Mr. Williams) for access to the field site; Richard Smith and Simon Tait of the Department of Civil Engineering, Sheffield University, for assistance in constructing the ADV wading rod; Ben Surridge, Louise Sime, Barry Hankin, and David Mould for assistance with fieldwork; and Andy Hodskinson for the topographic data for bend 37. Two anonymous reviewers and an associate editor provided constructive criticism that has greatly improved the final version of the paper.

References

Ashmore, P. E., R. I. Ferguson, K. L. Prestegaard, P. J. Ashworth, and C. Paola, Secondary flow in anabranch confluences of a braided, gravel-bed stream, *Earth Surf. Processes Landforms*, *17*, 299–311, 1992.

Bathurst, J. C., C. R. Thorne, and R. D. Hey, Secondary flow and shear stress at river bends, *J. Hydraul. Div. Am. Soc. Civ. Eng.*, *105*, 1277–1295, 1979.

Biron, P., B. de Serres, A. G. Roy, and J. L. Best, Shear layer turbulence at an unequal depth channel confluence, in *Turbulence: Perspectives on Flow and Sediment Transport*, edited by N. J. Clifford, J. R. French, and J. Hardisty, pp. 197–213, John Wiley, Hoboken, N. J., 1993.

Booker, D. J., D. A. Sear, and A. J. Payne, Modelling three-dimensional flow structures and patterns of boundary shear stress in a natural pool-riffle sequence, *Earth Surf. Processes Landforms*, *26*, 553–579, 2001.

Bradbrook, K. F., P. M. Biron, S. N. Lane, K. S. Richards, and A. G. Roy, Investigation of controls on secondary circulation in a simple confluence geometry using a three-dimensional numerical model, *Hydrol. Processes*, *12*, 1371–1396, 1998.

Bradbrook, K. F., S. N. Lane, and K. S. Richards, Numerical simulation of three-dimensional, time-averaged flow structure at river channel confluences, *Water Resour. Res.*, *36*, 2731–2746, 2000a.

Bradbrook, K. F., S. N. Lane, K. S. Richards, P. M. Biron, and A. G. Roy, Large eddy simulation of periodic flow characteristics at river channel confluences, *J. Hydraul. Res.*, *38*, 207–215, 2000b.

Czernuszenko, W., and A. A. Rylov, A generalisation of Prandtl's model for 3D open channel flows, *J. Hydraul. Res.*, *38*, 133–139, 2000.

Dietrich, W. E., and J. D. Smith, Influence of the point bar on flow through curved channels, *Water Resour. Res.*, *19*, 1173–1192, 1983.

Frothingham, K. M., and B. L. Rhoads, Three-dimensional flow structure and channel change in an asymmetrical compound meander loop, Embarras River, Illinois, *Earth Surf. Processes Landforms*, *28*, 625–644, 2003.

Hardy, R. J., S. N. Lane, R. I. Ferguson, and D. R. Parsons, Assessing the credibility of a series of computational fluid dynamics simulations of open channel flow, *Hydrol. Processes*, *17*, 1539–1560, 2003.

Hodskinson, A., and R. I. Ferguson, Numerical modelling of separated flow in river bends: Model testing and experimental investigation of geometric controls on the extent of flow separation at the concave bank, *Hydrol. Processes*, *12*, 1323–1338, 1998.

Huang, J., L. J. Weber, and Y. G. Lai, Three-dimensional numerical study of flows in open-channel junctions, *J. Hydraul. Eng.*, *128*, 268–280, 2002.

Lane, S. N., and K. S. Richards, The "validation" of hydrodynamic models: Some critical perspectives, in *Model Validation: Perspectives in Hydrological Science*, edited by M. G. Anderson and P. D. Bates, pp. 413–438, John Wiley, Hoboken, N. J., 2001.

Lane, S. N., P. M. Biron, K. F. Bradbrook, J. B. Butler, J. H. Chandler, M. D. Crowell, S. J. McLelland, K. S. Richards, and A. G. Roy, Three-dimensional measurement of river channel flow processes using acoustic Doppler velocimetry, *Earth Surf. Processes Landforms*, *23*, 1247–1267, 1998.

Lane, S. N., K. F. Bradbrook, K. S. Richards, P. A. Biron, and A. G. Roy, The application of computational fluid dynamics to natural river channels: Three-dimensional versus two-dimensional approaches, *Geomorphology*, *29*, 1–20, 1999.

Lane, S. N., K. F. Bradbrook, K. S. Richards, P. M. Biron, and A. G. Roy, Secondary circulation cells in river channel confluences: Measurement artefacts or coherent flow structures?, *Hydrol. Processes*, *14*, 2047–2071, 2000.

Launder, B. E., and D. B. Spalding, The numerical computation of turbulent flows, *Comput. Methods Appl. Mech. Eng.*, *3*, 269–289, 1974.

Leeder, M. R., and P. H. Bridge, Flow separation in meander bends, *Nature*, *253*, 338–339, 1975.

Leopold, L. B., R. A. Bagnold, M. G. Wolman, and L. M. Brush, Flow resistance in sinuous and irregular channels, *U.S. Geol. Surv. Prof. Pap.*, *282D*, 111–134, 1960.

Leschziner, M. A., and W. Rodi, Calculation of strongly curved open channel flow, *J. Hydraul. Eng.*, *105*, 1297–1314, 1979.

Lien, F. S., and M. A. Leschziner, Application of an RNG turbulence model to flow over a backwards-facing step, *Comput. Fluids*, *23*, 983–1004, 1994.

Meselhe, E. A., and F. Sotiropolous, Three-dimensional numerical model for open channels with free surface variations, *J. Hydraul. Res.*, *38*, 115–121, 2000.

Nicholas, A. P., and G. H. S. Smith, Numerical simulation of three-dimensional flow hydraulics in a braided channel, *Hydrol. Processes*, *13*, 913–929, 1999.

Pantankar, S. V., and D. B. Spalding, A calculation procedure for heat, mass and momentum transport in three-dimensional parabolic flows, *Int. J. Heat Mass Transf.*, *15*, 1787–1806, 1972.

Parsons, D. R., Flow separation in meander bends, Ph.D. thesis, 294 pp., Dep. of Geogr., Sheffield Univ., Sheffield, U. K., 2003.

Rhoads, B. L., and S. T. Kenworthy, Flow structure at an asymmetrical stream confluence, *Geomorphology*, *11*, 273–293, 1995.

Rhoads, B. L., and S. T. Kenworthy, On secondary circulation, helical motion and Rozovskii-based analysis of time-averaged two-dimensional velocity fields at confluences, *Earth Surf. Processes Landforms*, *24*, 369–375, 1999.

Rhoads, B. L., and A. N. Sukhodolov, Field investigation of three-dimensional flow structure at stream confluences: 1. Thermal mixing and time-averaged velocities, *Water Resour. Res.*, *37*, 2393–2410, 2001.

Roache, P. J., Quantification of uncertainty in computational fluid dynamics, *Annu. Rev. Fluid Mech.*, *29*, 123–160, 1997.

Rozovskii, I. L., *Flow of Water in Bends of Open Channels* (in Russian), Acad. of Sci. of the Ukrainian SSR, Kiev, 1957. (English translation, Isr. Program for Sci. Transl., Jerusalem, 1961.)

Sofialidis, D., and P. Prinos, Turbulent flow in open channels with smooth and rough floodplains, *J. Hydraul. Res.*, *37*, 615–640, 2000.

Sukhodolov, A. N., and B. L. Rhoads, Field investigation of three-dimensional flow structure at stream confluences: 2. Turbulence, *Water Resour. Res.*, *37*, 2411–2424, 2001.

Thorne, C. R., and R. D. Hey, Direct measurements of secondary currents at a river inflexion point, *Nature*, *280*, 226–228, 1979.

Thorne, C. R., and S. Rais, Direct measurement of secondary currents in a meandering sand-bed river, *Nature*, *315*, 746–747, 1985.

Van Alphen, J. S. L. J., P. M. Bloks, and P. Hoekstra, Flow and grainsize pattern in a sharply curved river bend, *Earth Surf. Processes Landforms*, *9*, 513–522, 1984.

Yakhot, V., and S. A. Orszag, Renormalization group analysis of turbulence, *J. Sci. Comput.*, *1*, 536–551, 1986.

Yakhot, V., S. A. Orszag, S. Thangham, T. B. Gatshi, and C. G. Speziale, Development of a turbulence model for shear flow by a double expansion technique, *Phys. Fluids A*, *4*, 1510–1520, 1992.

R. I. Ferguson, Department of Geography, University of Sheffield, Sheffield S10 2TN, UK. (r.ferguson@sheffield.ac.uk)

R. J. Hardy and S. N. Lane, School of Geography, University of Leeds, Leeds LS2 9JT, UK.

D. R. Parsons, Department of Earth Sciences, University of Leeds, Leeds LS2 9JT, UK.